Estimating global ocean heat content changes in the upper 1800 m since 1950 and the influence of climatology choice*

John M. Lyman[1]
Joint Institute for Marine and Atmospheric Research, University of Hawaii at Manoa, Honolulu, Hawaii, and NOAA/Pacific Marine Environmental Laboratory, Seattle, Washington

Gregory C. Johnson
NOAA/Pacific Marine Environmental Laboratory, Seattle, Washington

Submitted to *Journal of Climate*

11 October 2012

* Pacific Marine Environmental Laboratory Contribution Number 3884 and Joint Institute for Marine and Atmospheric Research Contribution Number 12-380.
[1] *Corresponding author address*: John Lyman, NOAA/Pacific Marine Environmental Laboratory, 7600 Sand Point Way N.E., Bldg. 3, Seattle, Washington 98115-6349, U.S.A.
E-mail: John.Lyman@noaa.gov

Abstract

The historical record of global ocean temperature measurements has improved over the years. Measurement depths have increased, spatial and temporal coverage has improved, and measurement techniques have advanced from decade to decade. Here ocean heat content anomalies are analyzed from 1950–2011 in five depth layers (0–100, 100–300, 300–700, 700–900, and 900–1800 m) that correspond to historic shifts in common maximum sampling depths of ocean temperature measurement instruments (mechanical bathythermograph - MBT, shallow expendable bathythermograph - XBT, deep XBT, early sometimes shallower Argo profiling floats, and recent Argo floats capable of worldwide sampling to 2000 m). This vertical separation of maps allows computation of annual ocean heat content anomalies and their sampling uncertainties back to 1950 while taking account of in situ sampling advances and changing sampling patterns. Global ocean heat uptake estimates since 1950 depend strongly on assumptions made concerning changes in undersampled or unsampled ocean regions. If unsampled areas are assumed to have zero anomaly, the choice of climatological reference from which anomalies are estimated can strongly influence the global integral values and their trend if global integrals are attempted in sparsely sampled times.

1. Introduction

The world's oceans have absorbed roughly 90% of the anthropogenic warming from greenhouse gasses since the 1960's (Bindoff et al. 2007). This well documented ocean warming occurs primarily in the upper 0–700 m (Domingues et al. 2008, Ishii and Kimoto 2009, Levitus et al. 2009), but warming has also been observed at intermediate and mid-depths, from 700–2000 m (von Schuckmann et al. 2009, Levitus et al. 2012), and in the abyssal ocean, well below 2000 m (Purkey and Johnson 2010, Kouketsu et al. 2011).

Historically, ocean temperature sampling is inhomogeneous both by geographic region and depth from year to year, with major shifts in observing techniques from decade to decade (Johnson and Wijffels 2011). Accurate but spatially sparse temperature measurements, sometimes to full depth, started after 1874 using reversing thermometers, gradually replaced, starting in the 1960s, with conductivity-temperature-depth (CTD) instruments. Starting in the 1930s mechanical bathythermographs (MBTs) made it easier to measure the upper ocean temperature (sampling as deep as 145 to 300 m, more often shallower than deeper). They were widely used in the 1950s and 1960s. Starting in 1966, the expendable bathythermograph (XBT) began to replace the MBT for upper ocean thermal sampling, with shallow XBTs (sampling as deep as 460 m) dominant in the 1970s and 1980s, and deep XBTs (sampling as deep as 760 m) dominant in the 1990s. Like MBTs, XBTs are not very accurate (nominally ±0.1°C for temperature and ±2% for depth), but both comprise a large part of the modern observational record of upper ocean

temperatures. The profiling CTD floats of the Argo Program (Roemmich et al. 2010) began to provide accurate, year-round sampling of upper ocean temperature starting in 2000. The array started regionally, but became near-global and largely replaced the XBT for distributed ocean measurements by 2005. Early on, some of the floats only sampled to around 1000 m, but as time goes on, more floats sample as deep as the 2000-m Argo target.

For climate studies, ocean temperature data are used to estimate ocean heat content anomalies (OHCA). There are many sources of uncertainty in estimates of annual global integrals of OHCA. While reversing thermometers and CTDs are relatively accurate, XBTs have biases in both depth and temperature; different choices of XBT bias corrections lead to large uncertainties from at least 1993 to 2008 (Lyman et al. 2010). Mechanical bathythermograph (MBT) bias corrections are equally important in earlier years (Gouretski and Reseghetti 2010, Ishii et al. 2009). Sampling uncertainty also contributes significantly to the overall uncertainty, and has strong dependence on time (Lyman and Johnson 2008, Domingues et al. 2008, Palmer and Brohan 2011) with larger uncertainties occurring for earlier years when the global ocean is not well sampled. Finally, uncertainties from mapping choices and climatology choice also contribute to the overall uncertainty. Mapping is sometimes done by bin averaging (Palmer et al. 2007, Gouretski et al. 2012), objective analysis (Ishii et al. 2009, Levitus et al. 2009), or reduced-space optimal interpolation (Domingues et al. 2008).

Here we focus on how sparse irregular sampling and choice of climatalogical baseline affects estimates of the global integral of OHCA, relative to a monthly Argo-period climatology. We analyze five distinct depth layers (0–100, 100–300, 300–700,

700–900, and 900–1800 m) to capture the historical sampling patterns of MBTs, XBTs and Argo floats. Since profiles often terminate at depths slightly shallower than the nominal maximum instrument sampling depth, layer bottom depths are chosen somewhat shallower than the nominal maximal sampling depths of MBTs (100 vs. 145–300 m), shallow XBTs (300 vs. 460 m), deep XBTs (700 vs. 760 m), and Argo floats (900 and 1800 vs. 2000 m) to maximize the number of profiles spanning each layer yearly.

We use sea surface height (SSH) as a proxy to estimate the OHCA sampling error in each of the depth intervals following Lyman and Johnson (2008). We quantify the effects of infilling on the global integral of OHCA by performing two integrations. One assumes zero anomalies in unsampled regions (mean of the maps) and the other that unsampled regions have anomalies equal to the average anomaly of sampled region (representative mean). We also discuss how choices of baseline climatology can modify the effects of infilling assumptions on the global OHCA estimates.

2. Data

This study uses two sources of data. The Hadley Centre observational dataset EN3_v2a (Ingleby and Huddleston 2007) is used with XBT and MBT bias corrections of Ishii and Kimoto (2009) applied. All the profiling float data are removed from this dataset, leaving data from temperature profiles from bottle-station reversing thermometers, CTDs, XBTs, MBTs, and moorings. Profiling float data are obtained from the U.S. Argo Global Data Acquisition Center (GDAC), removing floats with possible pressure drifts (Baker et al. 2011). Delayed-mode data are used when available, otherwise real-time data are used. Only data with quality flags of "good" are retained.

We apply additional quality control when computing OHCA to ensure that each layer is adequately sampled. Profiles that do not extend to the bottom depth of a given layer are not considered for that layer. Furthermore, for data from a profile to be used in any given layer, its mean vertical measurement spacing must on average be closer than twice the spacing of NODC World Ocean Atlas standard levels from 0–100 m, and closer than three times the standard level spacing below 100 m.

3. Method

OHCA and its sampling uncertainty are computed following Lyman and Johnson (2008). Aside from the quality control steps mentioned above, the other major differences are that OHCA is referenced to a seasonally varying Argo climatology and that both the OHCA and its sampling uncertainty are computed for 5 distinct depth layers (0–100, 100–300, 300–700, 700–900, and 900–1800 m) as detailed below. We discuss curves of the global integral of OHCA for 0–100, 0–300, 0–700, 0–900, and 0–1800-m layers. We compute these curves by adding the global integrals of OHCA for the appropriate sets of mapped layers.

a. OHCA mapping

Heat content in each of the 5 distinct layers is computed first for every profile. A new climatology of heat content with monthly resolution is computed using Argo data from 2005 to 2010 and removed from the heat content profiles to generate anomalies for each layer adequately sampled by the profiles. The results are then objectively mapped using a covariance function with both a large (~1000 km) scale and a small (~100 km) scale (Willis et al. 2004, Lyman and Johnson 2008).

b. Global integral of OHCA

We examine two simple assumptions that can be made when computing a global integral of OHCA, again following Lyman and Johnson (2008). The first assumption is that anomalies are zero in regions that are not sampled (mean of the maps). This sort of assumption is commonly used when integrating objective maps (e.g., Ishii et al. 2009, Levitus et al. 2012), and sometimes when summing bin-averaged data over the globe (Gouretski et al. 2012). The second assumption is that the anomalies in regions that are not sampled are the average of anomalies in sampled regions (representative mean), an assumption that has also been applied to global sums of bin-averaged data (Palmer et al. 2007). Since objective maps also tend to relax back to zero in areas that are undersampled, making a representative mean using an objective map is slightly more involved than doing so using bin averaged data. We apply the formalism of Lyman and Johnson (2008) to counteract that tendency of objective maps to relax to zero in data-poor regions when making a representative mean for an objective map. There are other methods for infilling gaps using satellite altimetry data either in an objective mapping formalism (Willis et al. 2004) or with reduced-space optimal interpolation (Domingues et al. 2008), but we do not address them here.

c. Sampling uncertainty of global OHCA integrals

Sampling uncertainties are computed in each mapped layer by using Aviso SSH as a proxy for OHCA (Lyman and Johnson 2008). Distinct spatially varying correlation coefficients are computed between SSH and the OHCA content for each mapped layer. When spatially integrating the SSH proxy of OHCA areas that were not sampled are

assumed to have the same anomalies as the area average anomaly of sampled regions. This representative mean yields an unbiased estimate of the global integral of Aviso SSH, bolstering confidence in the sampling uncertainties obtained by the method (Lyman and Johnson 2008).

When adding sampling uncertainties of the distinct depth layers, uncertainties are assumed correlated in areas where both layers are sampled and assumed uncorrelated if sampling areas in different layers do not overlap (Appendix A).

d. Climatology baseline shifts

We use a climatology based on Argo data because of Argo's even sampling throughout the year and its near-global spatial coverage of the upper 2000 m of the world's oceans. However, the resulting climatology is a modern (2005–2010) one, and thus almost certainly warmer than a long-term mean over our analysis period or conditions in say, 1950 (as far back in time as estimates are attempted here). Given the sparse sampling, how would the global integrals change if a different, colder, climatology were used?

We investigate that question by introducing a second climatology, which is just the Argo climatology with values shifted uniformly by a global representative mean estimate of heat content anomaly for each distinct layer in 1950. This shifted Argo climatology is considerably colder than the modern Argo climatology. The representative mean global average heat content anomaly for each layer in 1950 is computed from the 1950 heat content anomaly maps using the modern Argo climatology. The better to compare the resulting OHCA curves, the spatially integrated representative mean global average heat content anomaly from 1950 is added back to the OHCA curves estimated using the shifted colder Argo climatology.

4. Historical sampling

The historical record of vertical and horizontal structure of ocean temperature sampling is linked to the history of instrument development. The first world-wide survey of upper ocean temperatures, completed with min-max thermometers, was taken during the Challenger expedition in 1872–1876. Those data have recently been compared to Argo float data from the 2004–2010, finding statistically significant ocean warming over the intervening time interval (Roemmich et al. 2012). The development of the reversing thermometer in 1874 allowed measurement of temperature and depth over full ocean depths to a maximum accuracy of about 0.01ºC and 0.5%,respectively (Warren 2008). However, reversing thermometers require a ship to stop, and historical measurements prior to the International Geophysical Year (1957–1958) are globally very sparse (Boyer et al. 2009).

The development of the MBT circa 1938 allowed measurements from a moving ship, although the ship had to slow to a few knots underway for best results, profiles were no deeper than 300 m, often only to 100 m or so, and temperature accuracy was probably not as good as the stated 0.1ºC (Emery and Thomson 1998). MBT depth accuracy is at best 1% (Gouretski and Reseghetti 2010). Nonetheless, MBT profiles are the predominant upper ocean temperature observations from circa 1950 to 1969 (e.g., Johnson and Wijffels 2011). Their extensive use in northern hemisphere in the Pacific and Atlantic Ocean during that time period is evident in the average yearly 0–100-m layer sampling density (Fig. 1a). Bottle measurements that can extend below 1800 m in these same regions are far less extensive from 1950–1969 (Fig. 1e; i; m). The annual sampling density of the 0–100-m layer exceeds 50% starting in 1957 (Fig. 2). The widespread use

of the MBT allows that 50% sampling benchmark to be reached at this early date, but only for the uppermost layer.

From circa 1970 to 1989 shallow XBTs, profiling as deep as 460 m, are predominant contributors to the historical temperature record (e.g., Boyer et al. 2009; Johnson and Wijffels 2011). Accuracies of ±0.1ºC and ±2% for temperature and depth, respectively, are specified for the XBT, but systematic, time-dependent biases can approach or exceed these values (e.g., Gouretski and Reseghetti 2010). The use of the shallow XBT coincides with well-measured temperature (on an annual basis) in the northern Hemispheres of all three oceans (now including the Indian Ocean) and extending to the 100–300 m layer (Fig. 1b; f). The southern hemisphere subtropics are also somewhat better, although still inadequately (in terms of annual averages) measured in these layers during this time. Reversing thermometer and CTD data collected during this period increase temperature sampling in the 300–700, 700–900, and 900–1800 m layers (Fig. 1l; n). The annual sampling density of the 100–300-m layer exceeds 50% starting in 1967 (Fig. 2), as a result of the commencement of widespread use of the shallow XBT starting around that time.

Deeper XBTs (measuring frequently to at least 700 m; with measurement accuracies and biases similar to the shallow XBTs; e.g., Gouretski and Reseghetti 2010), while introduced earlier, become an important source of historical temperature data from circa 1990 to 2004 (e.g., Johnson and Wijffels 2011) during and after the World Ocean Circulation Experiment (WOCE). During this time period adequate sampling extends into the Southern Hemisphere subtropics of all three oceans, even to the 300–700-m layer (Fig 1c; g; k). The annual sampling density of the 300–700-m layer exceeds 50%

starting in 1983 (Fig. 2), as a result of the increasingly widespread use of the deep XBT during the pre-WOCE large-scale measurement programs. This coverage to 700 m peaks at a local temporal maximum of around 79% in 1994 and then declines to a local temporal maximum of 63% in 2001 partly because some XBT data are slow to filter into the data archival centers, and partly as a result of difficulties sustaining gains in ocean observations at the end of WOCE. Deep CTD stations occupied during WOCE further improve sampling in the 700–900 and 900–1800-m (Fig. 1o) layers (but still not adequately outside of the North Atlantic and western North Pacific Oceans). These layers also show a similar decline between 1993 and 2000 with the end of WOCE (Fig. 2).

The Argo program of autonomous profiling CTD floats (Roemmich et al. 2009) began sampling the upper half of the ocean (nominally to 2000 m) in the year 2000. These floats have nominal temperature accuracy of 0.02ºC, but usually much better, and nominal pressure (hence depth) accuracy of 0.12%. By 2005 (and through 2010 and beyond) Argo achieved near global coverage in the ice-free oceans excluding marginal seas down to 900 m (Fig. 1j). However, the tropics, with their very light surface waters, presented some challenges for early Argo floats, so not all of them could profile there much beyond 1000 m leaving that area slightly undersampled during 2005–2010 (Fig. 1p). As more capable floats that can profile from the surface to 2000 m even in the tropics replace the earlier, more limited, floats, that coverage gap is gradually being filled. The annual sampling density of the 700–900-m layer exceeds 50% starting in 2003 (Fig. 2). That same milestone is reached for the 900–1800-m layer starting in 2005

as a result of the increasingly capable and widespread Argo array. By 2010, over 80% of the global ice-free oceans are sampled even to 900–1800-m layer (Fig. 2).

Sampling of the ocean temperature below 2000 m (not treated here) is still very sparse, limited at present to shipboard CTDs. In most areas comparisons of co-located oceanographic sections (e.g., Purkey and Johnson 2010) or data assimilation into models (e.g., Kouketsu et al. 2011) may be the most appropriate way to assess decadal changes below 2000 m, although it is possible to map multi-decadal changes in ocean heat content in the North Atlantic (e.g. Lozier et al., 2008), historically the best-sampled ocean.

5. Climatologies and time-varying spatial coverage

The method used to globally integrate annual OHCA maps has a large impact on estimates of heat uptake since 1950 in the upper 0–1800 m of the global oceans. The mean of the maps referenced to a modern climatology (Fig. 3, dashed grey lines) yields a smaller overall rate of heat uptake since 1950 than the representative mean (Fig. 3, solid black lines) in all depth ranges considered. The mean of the maps integration referenced to a modern (presumably warm) climatology tends to relax back to zero when the data coverage for the layers integrated (Fig. 2) becomes sparse. This result occurs because the objective maps relax back to zero anomaly where data are sparse, zero anomaly in most locations will presumably tend to be on the warm side of the (poorly known) long-term average because the Argo climatology used is modern (2005–2010). In other words, the annual mean of the maps values using a modern climatology are pulled towards cooler values earlier in time by cooler temperature data, but for times when data are sparse, they relax back to the mean, which is warm owing to the modern climatology used.

One way to demonstrate this effect is to use a cooler climatology to produce contrasting curves for the global means of the maps (Fig. 3, black dashed lines). Here we simply shift the Argo climatology to the colder mean 1950 values estimated using the representative mean anomalies for each layer. This shift results in a much larger warming trend for the curves produced from mean of the maps than does the modern Argo climatology. This difference arises solely because the mean of the maps assumes zero anomalies in unsampled regions. With a climatology shifted to colder 1950 mean values, the large extents of the maps with sparse data in the early years all relax back to relatively colder 1950 mean values as a baseline, rather than the warmer Argo climatology values. In the more recent years, the larger sampled fraction of the global ocean (Fig. 2) means that the means of the maps for either the colder 1950s climatology or the warmer modern Argo climatology are more constrained by data to be similar (Fig. 3). Hence, for the mean of the maps, the changing and sometimes sparse sampling patterns combine with the climatology to produce trends that depend on the climatology values, especially if those trend estimates span times of sparse sampling.

Unlike the mean of the maps, the representative mean (Fig. 3, black solid line) is the same for both the Argo climatology shifted to 1950 values and the modern Argo climatology. This result holds because the representative mean avoids any relaxation back to climatological values by assuming that the mean anomaly of the sampled regions applies to the unsampled regions.

6. Sampling Uncertainty

Computing the global integral using the representative mean increases both the signal within and the noise from the observed areas of the global ocean by extending them to the

unmeasured areas (Lyman and Johnson 2008). The sampling uncertainty (Fig. 4), which generally grows as sampling becomes sparse (Fig. 2), is only one component of the total uncertainty (e.g., Lyman et al. 2010). Here we do not concern ourselves with other contributions, but there is much work being done by the larger community on quantifying uncertainties remaining in XBT and MBT bias corrections, as well as those owing to differences in quality control, mapping, and climatology.

Sampling uncertainty (Fig. 4) increases greatly with decreased area coverage (Fig. 2), so it ramps up prior to about 1956 in the 0–100-m layer. After that date MBT use expanded, around the time of the International Geophysical Year (IGY). The advent of the IGY further reduces sampling uncertainties in all layers because of a rise in reversing thermometer data from deep oceanographic stations. The sampling uncertainty for 0–300 m declines further after around 1969, with the increasingly widespread use of the shallow XBT, and decreases markedly for 0–700 around 1990, with the more widespread use of the deep XBT and the advent of WOCE. Again, WOCE reduces sampling error in all layers during the 1990s, because of increased CTD stations worldwide. However, around the year 2000, there is a slight increase in sampling error in all layers as WOCE sampling wound down before Argo sampling spun up. Starting around 2001–2003, sampling errors in all layers begin to shrink, reaching a historical low by 2005–2006, depending on the depth of integration, and remaining small as Argo coverage continues to improve.

Sampling uncertainties (Fig. 4) generally decrease as areal coverage (Fig. 2) increases. This inverse relationship is not perfect, at least partly because OHCA variance is spatially variable, so increasing sampling in one region might reduce sampling error

more than increasing it the same amount in another region. Furthermore, the contribution to sampling error in deeper layers is relatively small even though the area sampled is also small except in recent years. This situation likely holds owing to the decreasing heat content anomaly signals of eddies, planetary waves, gyre shifts, and even warming, with increasing depth.

7. Discussion

Ocean warming is observed between 1950 and 2011 in all layers for both methods of global integration: mean of the maps or representative means (Fig. 3). However, the representative mean is more likely to result in an un-biased trend (Lyman and Johnson 2008). Furthermore, we show that the representative mean is insensitive to mean shifts in the background climatology, whereas the trends from means of the maps vary greatly depending on such shifts. For a modern (warmer) climatology, the mean of the maps values for early, poorly sampled years shift back toward zero anomaly (warm conditions), increasingly reducing the warming trend the further back in time that trend is computed. In contrast, for climatologies shifted to early (colder) values, the mean of the maps values for early years are cold, but appropriately warm in later years because the data coverage of the warmed oceans is improved in recent years. This difference results in a very different trend depending on the climatology for curves produced using means of the maps. While further analyses are needed to quantify the impacts of regional variability in climatologies (rather than the global shifts applied here) on the OHCA curves, representative averaging provides an estimate of the warming rate that doesn't depend on the mean heat content of the climatology.

Here we only compute and analyze sampling uncertainties. Before the significance of the trends in the global integral OHCA can be completely determined over various lengths of the historical record it will be necessary to examine other sources of uncertainty in more detail. These include uncertainties owing to quality control, choice of XBT and MBT bias correction, choice of climatology, and choice of mapping method. Nonetheless, when areal coverage gets smaller, OHCA sampling uncertainties generally get larger. There is a roughly inverse relationship between these quantities in each layer, with smaller and smaller contributions of the error per unit depth with increasing depth (not shown). Of course, the warming signal in the upper 1800 m also gets smaller per unit depth with increasing depth (e.g., Johnson and Wijffels 2011). The 50% coverage benchmark (Fig. 3, vertical lines) discussed above for the different layers is arbitrary, but a reminder that below some areal coverage, it becomes difficult to make a realistic estimate of the global integral OHCA for a given year in a given layer, no matter the mapping method.

Finally, while XBT biases have received much attention in the last few years, MBTs are a large source of upper ocean temperature data from the 1950s through the 1960s, and their biases have been estimated by only a few investigators (e.g., Gouretski and Reseghetti 2010, Ishii et al. 2009). Sampling errors on the representative mean during this time period are large (Fig. 4), however the warming signal also large (Fig. 3). In order to determine if this large signal is statistically significant it will be necessary to estimate all possible sources of uncertainty, including uncertainties in MBT bias corrections.

Acknowledgments.

Altimeter products used herein were produced by SSALTO/DUACS as part of the Environment and Climate EU Enact project (EVK2–CT2001–00117) and distributed by AVISO, with support from CNES. The bulk of the in situ data used herein was provided Hadley Centre (www.metoffice.gov.uk/hadobs). Float data were collected and made freely available by the Argo Program (of the Global Ocean Observing System) and contributing national programs (http://www.argo.net/). The NOAA Climate Program Office and the NOAA Office of Oceanic and Atmospheric Research provided support for this research. The findings and conclusions in this article are those of the authors and do not necessarily represent the views of the National Oceanic and Atmospheric Administration.

APPENDIX A

Summation of Uncertainty

Addition of Sampling Uncertainty from the surface

In using Aviso SSH as a proxy for every depth layer of OHCA (following Lyman and Johnson 2008), we have implicitly assumed that eddy statistics of the upper layers are similar to deep layers.

We also make another assumption, that the correlated sampling uncertainties between depth layers i and j ($CorrSE_{ij}$) are proportional to the square root of the percentage change in the globe coverage for depth layer i (Δ_i) as a fraction of the total percentage of the globe sampled in depth layer j (f_j, Fig. 2). Hence the sampling error for a given depth layer j (SE_j) is

$$CorrSE_{ij} \equiv SE_j \sqrt{\frac{\Delta_i}{f_j}}, \qquad \text{(A1)}$$

where $\Delta_k \equiv f_k - f_{k-1}$. Note that $\Delta_{900-1800} = f_{900-1800}$, because it is the bottom layer and $\sum_{k=0-100}^{900-1800} \Delta_k = f_{0-100}$. Summing the correlated sampling uncertainties from the surface to the bottom of a given depth layer and then adding the resulting uncertainties in quadrature (thus assuming they are uncorrelated) yields:

$$SE_{0-depth\_layer} = \sqrt{\sum_{i=0-100}^{900-1800} \left(\sum_{j=0-100}^{depth\_layer} CorrSE_{ij} \right)^2}, \qquad \text{(A2)}$$

where $SE_{0-depth\_layer}$ is the sampling error from the surface to the bottom of the *depth_layer* of interest.

References

Barker, P. M., J. R. Dunn, C. M. Domingues, and S. E. Wijffels, 2011: Pressure sensor drifts in Argo and their impacts. *J. Atmos. Oceanic Tech.*, **28**, 1036–1049, doi:10.1175/2011JTECHO831.1.

Bindoff, N. L., and Coauthors, 2007: Observations: Oceanic climate change and sea level. *Climate Change 2007: The Physical Science Basis*, S. Solomon et al., Eds., Cambridge University Press, 385–432.

Boyer, T.P., and Coauthors, 2009: *World Ocean Database 2009.* S. Levitus, Ed., NOAA Atlas NESDIS 66, U.S. Gov. Printing Office, Wash., D.C., 216 pp., DVDs.

Domingues, C. M., J. A. Church, N. J. White, P. J. Gleckler, S. E. Wijffels, P. M. Barker, and J. R. Dunn, 2008: Improved estimates of upper-ocean warming and multi-decadal sea level rise. *Nature*, **453**, 1090–1094, doi:10.1038/nature07080.

Gouretski, V., J. Kennedy, T. Boyer, and A. Köhl, 2012: Consistent near-surface ocean warming since 1900 in two largely independent observing networks. *Geophys. Res. Lett.*, **39**, L19606, doi:10.1029/2012GL052975.

Gouretski, V., and F. Reseghetti, 2010: On depth and temperature biases in bathythermograph data: Development of a new correction scheme based on analysis of a global ocean database. *Deep-Sea Res. I*, **57**, 812–833, doi: 10.1016/j.dsr.2010.03.011.

Emery, W.J. and R.E. Thomson. 1998. *Data Analysis Methods in Physical Oceanography*. Elsevier, Oxford, 634 pp.

Ingleby, B., and M. Huddleston, 2007: Quality control of ocean temperature and salinity profiles - historical and real-time data. *J. Mar. Syst.*, **65**, 158–175, 10.1016/j.jmarsys.2005.11.019

Ishii, M., and M. Kimoto, 2009: Revaluation of historical ocean heat content variations with time-varying XBT and MBT depth bias corrections. *J. Oceanogr.*, **65**, 287–299 doi:10.1007/s10872-009-0027-7.

Johnson, G. C., and S. E. Wijffels, 2011: Ocean density change contributions to sea level rise. *Oceanogr.*, **24(2)**, 112–121, doi:10.5670/oceanog.2011.31.

Kouketsu, S., and Coathors, 2011: Deep ocean heat content changes estimated from observation and reanalysis product and their influence on sea level change. *J. Geophys. Res.*, **116**, C03012, doi:10.1029/2010JC006464.

Levitus, S., J. Antonov, and T. Boyer, 2005: Warming of the World Ocean, 1955–2003. *Geophys. Res. Lett.*, **32,** L02604,doi:10.1029/2004GL021592.

Levitus, S., J. I. Antonov, T. P. Boyer, R. A. Locarnini, H. E. Garcia, and A.V. Mishonov, 2009: Global ocean heat content 1955–2008 in light of recently revealed instrumentation problems. *Geophys. Res. Lett.*, **36**, L07608, doi:10.1029/2008GL037155.

Levitus, S., and Coauthors, 2012: World ocean heat content and thermosteric sea level change (0–2000 m), 1955–2010. *Geophys. Res. Lett.*, **39**, L10603, doi:10.1029/2012GL051106.

Lozier, M. S., S. J. Leadbetter, R. G. Williams, V. Roussenov, M. S. C. Reed and N. J. Moore, 2008: The spatial pattern and mechanisms of heat content change in the North Atlantic. *Science*, **319**, 800–803.

Lyman, J. M., and G. C. Johnson, 2008: Estimating annual global upper ocean heat content anomalies despite irregular in situ ocean sampling. *J. Climate*, **21**, 5629–5641, doi:10.1175/2008JCLI2259.1.

Lyman, J. M., S. A. Good, V. V. Gouretski, M. Ishii, G. C. Johnson, M. D. Palmer, D. M. Smith and J. K. Willis, 2010: Robust warming of the global upper ocean. *Nature*, **465**, 334–337, doi:10.1038/nature09043.

Palmer, M. D., K. Haines, S. F. B. Tett, and T. J. Hansell, 2007: Isolating the signal of ocean global warming. *Geophys. Res. Lett.*, **34**, L23610, doi: 10.1029/2007GL031712.

Palmer, M. D., and P. Brohan, 2011: Estimating sampling uncertainty in fixed-depth and fixed-isotherm estimates of ocean warming. *Int. J. Climatol.* **31**, 980–986, doi:10.1002/joc.2224.

Purkey, S. G., and G. C. Johnson, 2010: Warming of global abyssal and deep Southern Ocean between the 1990s and the 2000s: Contributions to global heat and sea level rise budgets. *J. Climate*, **23**, 6336–6351, doi:10.1175/2010JCLI3682.1.

Roemmich, D., and Coauthors, 2009: The Argo Program: Observing the global oceans with profiling floats. *Oceanogr.*, **22(2)**, 34–43.

Roemmich, D., W. J. Gould, and J. Gilson, 2012: 135 years of global ocean warming between the Challenger expedition and the Argo Programme. *Nature Climate Change*, **2**, 425–428, doi:10.1038/nclimate1461.

von Schuckmann, K., F. Gaillard, and P.-Y. L. Traon, 2009: Global hydrographic variability patterns during 2003–2008. *J. Geophys. Res*., **114**, C09007, doi:10.1029/2008JC005237.

Warren, B. A., 2008: Nansen-bottle stations at the Woods Hole Oceanographic Institution. *Deep-Sea Res. I*, **55**, 379–395, doi: /10.1016/j.dsr.2007.10.003.

Willis, J. K., D. Roemmich, and B. Cornuelle, 2004: Interannual variability in upper ocean heat content, temperature, and thermosteric expansion on global scales, *J. Geophys. Res.*, **109**, C12036, doi:10.1029/2003JC002260.

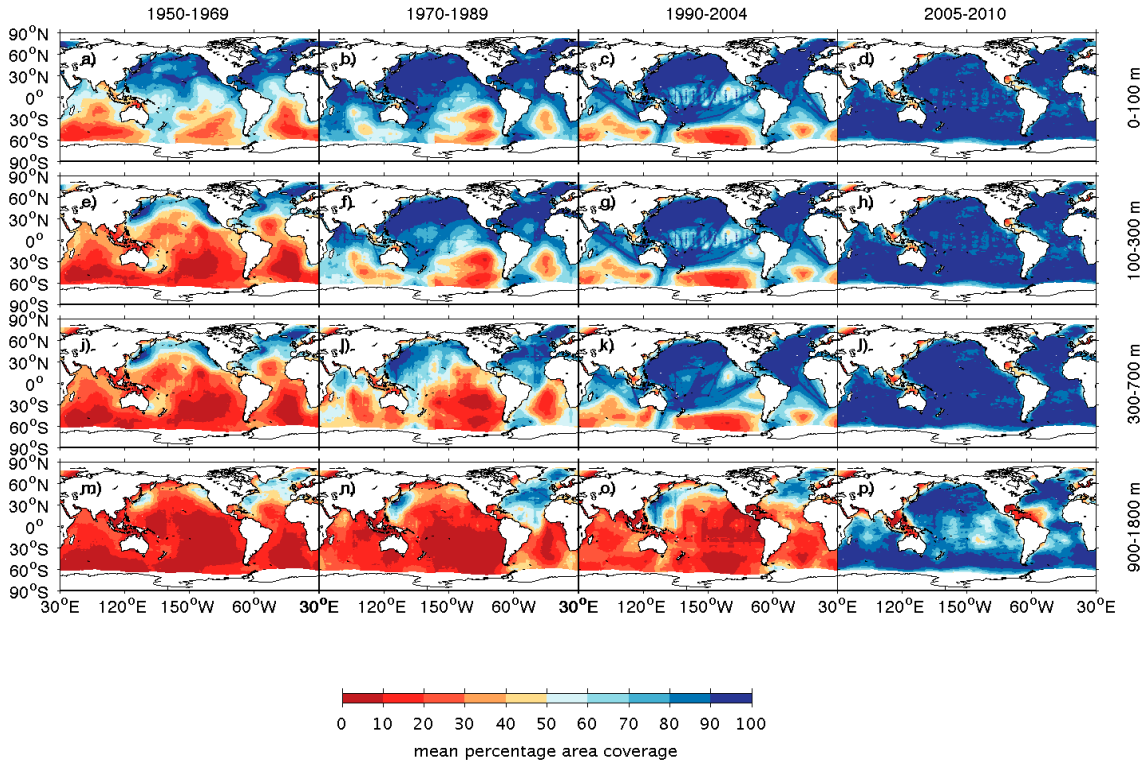

FIG. 1. Means of annual in situ temperature data sampling coverage (following Lyman and Johnson 2008) for various depth levels and time ranges. From top to bottom: 0–100 m, 100–300 m, 300–700 m, and 900–1800 m. From left to right: 1950–1969, 1970–1989, 1990–2004, and 2005–2010.

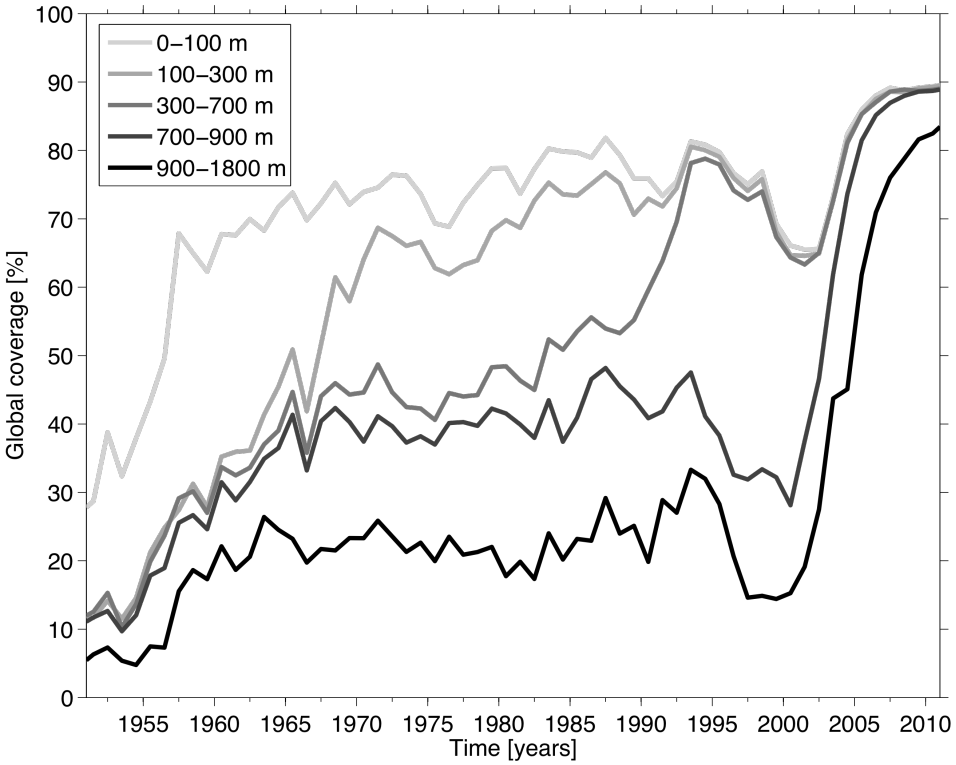

FIG. 2. Annual percentage of global ice-free ocean sampled for in situ ocean temperature (following Lyman and Johnson, 2008) for (proceeding from lightest grey to black lines) 0–100 m, 100–300 m, 300–700 m, 700–900 m, and 900–1800 m.

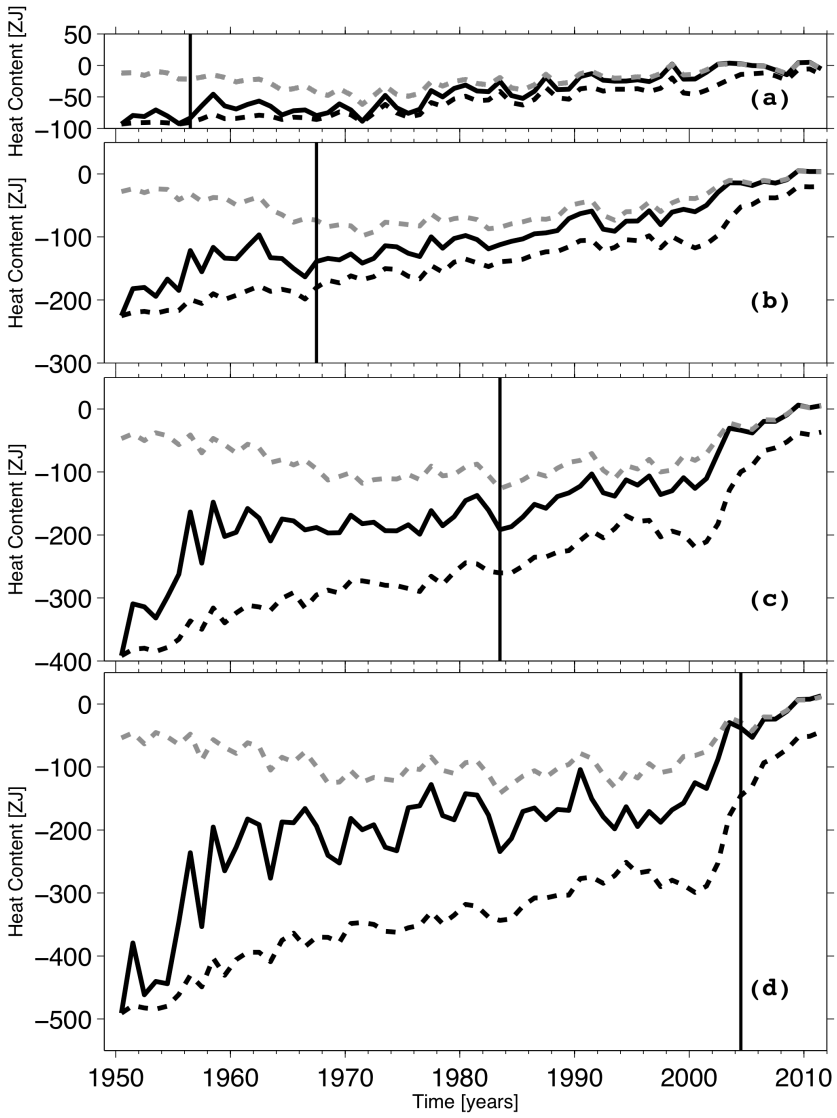

FIG. 3. Time series of annual average global integrals of upper ocean heat content anomaly (10^{21} J, or ZJ) for (a) 0–100 m, (b) 0–300 m, (c) 0–700 m, and (d) 0–1800 m. Time series are shown using simple means of the maps relative to both an Argo period climatology (dashed grey lines) and an Argo period climatology shifted to an 1950 mean (dashed black lines). Time series are also shown using representative means (black solid lines), which are not affected by shifts in the mean climatology. Thin vertical lines denote when the coverage (Fig. 2) reaches 50% for (a) 0–100 m, (b) 100–300 m, (c) 300–700 m, and (d) 900–1800 m.

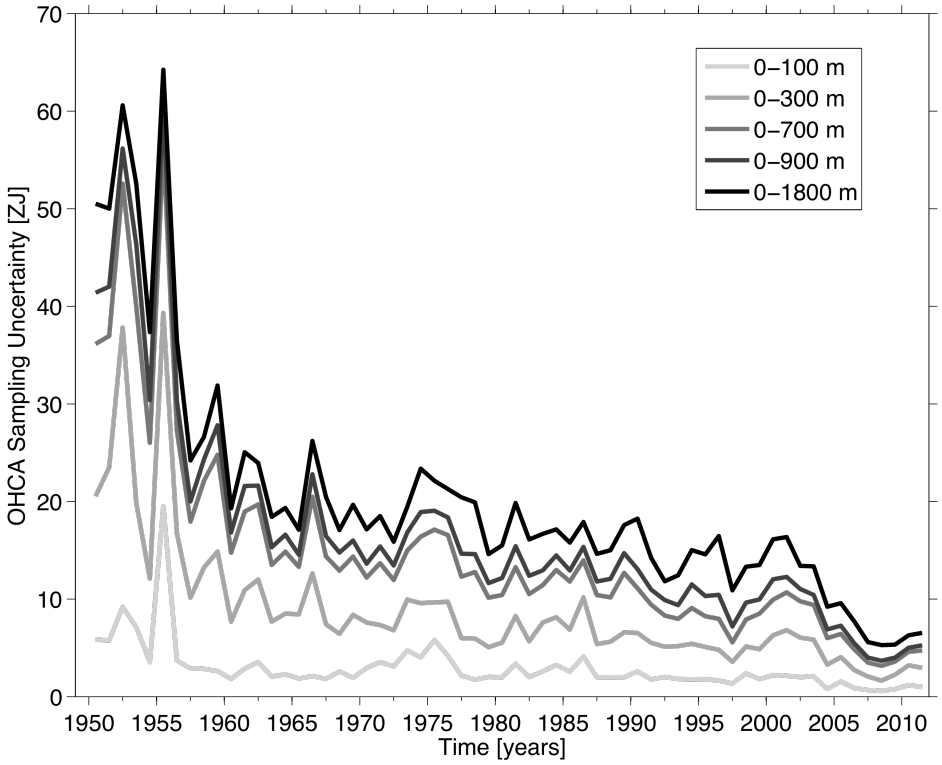

FIG. 4. Estimates of sampling uncertainties (following Lyman and Johnson, 2008) at one standard error of the mean for (proceeding from lightest grey to black lines) 0–100 m, 0–300 m, 0–700 m, 0–900 m, and 0–1800 m. Uncertainties are computed by summing up sampling uncertainties for each layer from the surface downwards. Where sampled layers overlap in space, uncertainties are added. Where sampled layers do not spatially overlap, uncertainties are summed in quadrature.